Clays and Clay Minerals, Vol. 64, No. 4, 389–400, 2016.

MOLECULAR SIMULATION OF CESIUM ADSORPTION AT THE BASAL SURFACE OF PHYLLOSILICATE MINERALS

Sebastien Kerisit[1]*, Masahiko Okumura[2], Kevin M. Rosso[1], and Masahiko Machida[2]

[1] Physical Sciences Division, Pacific Northwest National Laboratory, Richland, Washington 99354, USA
[2] Center for Computational Science and e-Systems, Japan Atomic Energy Agency, 5-1-5 Kashiwanoha, Kashiwa, Chiba 277-8587, Japan

Abstract—A better understanding of the thermodynamics of radioactive cesium uptake at the surfaces of phyllosilicate minerals is needed to understand the mechanisms of selective adsorption and help guide the development of practical and inexpensive decontamination techniques. In this work, molecular dynamics simulations were carried out to determine the thermodynamics of Cs^+ adsorption at the basal surface of six 2:1 phyllosilicate minerals, namely pyrophyllite, illite, muscovite, phlogopite, celadonite, and margarite. These minerals were selected to isolate the effects of the magnitude of the permanent layer charge ($\leqslant 2$), its location (tetrahedral *vs.* octahedral sheet), and the octahedral sheet structure (dioctahedral *vs.* trioctahedral). Good agreement was obtained with the experiments in terms of the hydration free energy of Cs^+ and the structure and thermodynamics of Cs^+ adsorption at the muscovite basal surface, for which published data were available for comparison. With the exception of pyrophyllite, which did not exhibit an inner-sphere free energy minimum, all phyllosilicate minerals showed similar behavior with respect to Cs^+ adsorption; notably, Cs^+ adsorption was predominantly inner-sphere, whereas outer-sphere adsorption was very weak with the simulations predicting the formation of an extended outer-sphere complex. For a given location of the layer charge, the free energy of adsorption as an inner-sphere complex varied linearly with the magnitude of the layer charge. For a given layer charge location and magnitude, adsorption at phlogopite (trioctahedral sheet structure) was much less favorable than at muscovite (dioctahedral sheet structure) due to electrostatic repulsion between adsorbed Cs^+ and the H atom of the OH^- ion directly below the six-membered siloxane ring cavity. For a given layer charge magnitude and octahedral sheet structure, adsorption to celadonite (octahedral sheet layer charge) was favored over adsorption to muscovite (tetrahedral sheet layer charge) due to the increased distance to the surface K^+ ions and the decreased distance to the O atom of the OH^- ion directly below the surface cavity.

Key Words—Adsorption Free Energy, Cesium, CLAYFF, Inner-Sphere, Layer Charge, Mica, Molecular Dynamics, Outer-Sphere, Potential of Mean Force, (001) Surface.

INTRODUCTION

On March 11, 2011, a catastrophic earthquake and ensuing tsunami hit Japan, causing massive devastation including, in particular, the partial meltdown of the cores of three operating nuclear reactors at the Fukushima Dai-ichi Nuclear Power Plant. As a result of this nuclear accident, large amounts of radioactive Cs were released and aerially deposited onto the topsoil of the surrounding Fukushima prefecture. Among many other phases, soils from the Fukushima prefecture contain phyllosilicate minerals including clay minerals, such as kaolinite and smectite, and micaceous minerals (Kozai *et al.*, 2012; Qin *et al.*, 2012). Due to the strong and selective interaction of Cs with phyllosilicate minerals, Cs contamination has, as expected, remained strongly associated with the topmost section of Fukushima soils (Kato *et al.*, 2012; Tanaka *et al.*, 2012). As a result, decontamination efforts by the Japanese government have focused on physical removal of contaminated top soils, a process that has generated significant waste soil volumes that have accumulated into temporary storage facilities and for which an efficient treatment procedure for waste volume reduction has yet to be developed and implemented.

An improved understanding of the microscopic mechanisms of adsorption and incorporation of Cs in phyllosilicate minerals is expected to provide a pathway for guiding the development of practical and inexpensive decontamination techniques. In particular, molecular simulations allow a given process to be studied in isolation and the effects of hypothesized controlling-factors to be determined and, as such, can provide a useful complement to experiments (Okumura *et al.*, 2013). In this work, molecular dynamics (MD) techniques were employed to study the effects of the permanent layer charge of phyllosilicate minerals on

* E-mail address of corresponding author:
sebastien.kerisit@pnnl.gov
DOI: 10.1346/CCMN.2016.0640405

This paper is published as part of a special issue on the subject of 'Computational Molecular Modeling'. Some of the papers were presented during the 2015 Clay Minerals Society-Euroclay Conference held in Edinburgh, UK.

Table 1. Force field parameters: Ionic charges.

Species	Charge (e)	Species	Charge (e)
Cesium (Cs)	1.000000	Oxygen – bridging (Ob)	−1.050000
Potassium (K)	1.000000	Oxygen – bridging with tetrahedral substitution (Obts)	−1.168750
Calcium (Ca)	2.000000	Oxygen – bridging with octahedral substitution (Obos)	−1.180833
Silicon – tetrahedral (St)	2.100000	Oxygen – hydroxyl (Oh)	−0.950000
Aluminum – tetrahedral (At)	1.575000	Oxygen – hydroxyl with substitution (Ohs)	−1.080833
Aluminum – octahedral (Ao)	1.575000	Hydrogen – hydroxyl (Ho)	0.425000
Magnesium – dioctahedral (Mgo)	1.360000	Oxygen – water (O*)	−0.820000
Magnesium – trioctahedral (Mgh)	1.050000	Hydrogen – water (H)	0.410000

Symbols for Si, Al, Mg, O, and H species taken from Cygan *et al*. (2004).

Cs adsorption. Permanent layer charges are created by the substitution of tetrahedral and/or octahedral cations for cations with a different valence. Micaceous minerals can differ in layer charge location (tetrahedral sheet *vs.* octahedral sheet) and magnitude ($\leqslant 2$). Both factors can significantly impact Cs uptake and release, as illustrated in previous work (Okumura *et al.*, 2013; 2014; Rosso *et al.*, 2001); however, no systematic analysis has been performed to date to comprehensively determine the magnitude of these effects. This work endeavored to determine the free energy profiles for Cs adsorption on a series of model phyllosilicate minerals with different permanent layer charge locations and magnitudes. The effort was concentrated on Cs^+ adsorption onto basal surfaces as an entry point to understand the behavior of the ion-exchangeable surface area fraction of these minerals. The effects of other phyllosilicate characteristics, such as interlayer water or cation mixtures, both tetrahedral and octahedral sheet substitutions, clay swelling, *etc.* are beyond the scope of the present study and will be considered in future work.

COMPUTATIONAL METHODS

Molecular dynamics simulations

The MD simulations were carried out with the computer program DL_POLY (Smith and Forester, 1996). In these simulations, atoms were represented as point-charge particles that interact through long-range Coulombic forces and short-range interactions. The latter were described by parameterized functions and represented the repulsion between electron-charge clouds, van der Waals attraction forces, and many-body terms, such as bond angle bending. The force field parameters employed in this work were those of the CLAYFF force field (Cygan *et al.*, 2004), which uses the flexible SPC model to simulate water molecules, and are listed in Table 1 (ionic charges) and Table 2 (short-range parameters).

The MD simulations of bulk phyllosilicates were performed in the NPT ensemble (constant number of particles, constant pressure, and constant temperature), whereas the simulations of the phyllosilicate mineral–water interface were performed in the NVT ensemble (constant number of particles, constant volume, and constant temperature). All the calculations were performed at 300 K and zero applied pressure. The temperature and pressure were kept constant by use of the Nosé-Hoover thermostat (Hoover, 1985) and Hoover barostat (Melchionna *et al.*, 1993), respectively. The electrostatic interactions were calculated by means of the Ewald summation method (Ewald, 1921). A 10 Å cutoff was used for the short-range interactions and the real part of the Ewald sum. The Ewald sum parameters were chosen to achieve a relative electrostatic energy error of at most 10^{-7}. The Verlet leapfrog algorithm was used to integrate the equations of motion with a time step of 1 fs.

Model phyllosilicates

Six model 2:1 phyllosilicates, namely pyrophyllite, illite, muscovite, phlogopite, celadonite, and margarite, were considered in this work to investigate the effects of

Table 2. Force field parameters: Short-range interactions.[a]

	D_0 (kJ/mol)[b]	R_0 (Å)[b]
Cs	4.18×10^{-1}	4.3002
K	4.18×10^{-1}	3.7423
Ca	4.18×10^{-1}	3.2237
St/At	7.70×10^{-6}	3.7064
Ao	5.56×10^{-6}	4.7943
Mgo/Mgh	3.78×10^{-6}	5.9090
O (all species)	6.50×10^{-1}	3.5532

[a] Also include the o*-h* and oh/ohs-ho harmonic bond stretch terms ($V_{ij} = k_1/2(r_{ij}\text{-}r_0)^2$ where k_1 = 4637.0 kJ/mol/Å^2 and r_0 = 1 Å) and the h*-o*-h* harmonic angle bend term ($V_{ijk} = k_2/2(\theta_{ijk}-\theta_0)^2$ where k_2 = 383.0 kJ/mol/rad^2 and θ_0 = 109.47°). See Table 1 for definition of St, At, Ao, Mgo, and Mgh.

[b] Functional form: $V_{ij} = D_{0,ij}[(R_{0,ij}/r_{ij})^{12}-2(R_{0,ij}/r_{ij})^6]$ with $D_{0,ij} = \sqrt{(D_{0,i} \times D_{0,j})}$ and $R_{0,ij} = 1/2(R_{0,i} + R_{0,j})$.

https://doi.org/10.1346/CCMN.2016.0640405 Published online by Cambridge University Press

layer charge magnitude and location on Cs adsorption energetics at the basal surface as well as the effect of octahedral sheet structure (*i.e.* dioctahedral *vs.* trioctahedral). The chemical formulae, structures, and layer charge magnitude and location of the six model phyllosilicates are given in Table 3. The structure and compositions used in this work were simplified model phyllosilicates. In other words, idealized stoichiometries were used with only one interlayer cation, only Al substitution in both the tetrahedral and octahedral sheets, and no F^- substitution for OH^-. In addition, Al substitutions were arranged in regular patterns (Figure 1). This approach was employed to facilitate isolating the effects of the structural properties of interest, namely the permanent charge magnitude and location as well as the octahedral sheet structure. Following this approach, the idealized illite structure S7 studied with *ab initio* methods by Hernández-Laguna *et al.* (2006) and Geatches and Wilcox (2014) was used, which consisted of a single Al substitution for Si in the tetrahedral sheet that is charge-compensated by a K^+ interlayer cation.

The series pyrophyllite, illite, muscovite, and margarite allowed determination of the effects of layer charge magnitude on Cs adsorption for a tetrahedral sheet layer charge and 2:1 dioctahedral sheet structure. Additionally, the comparison between muscovite and phlogopite allowed determination of the effects of octahedral sheet structure for a −1 layer charge located in the tetrahedral sheet. Finally, the comparison between muscovite and celadonite allowed a determination of the effects of layer charge location for a −1 layer charge and a 2:1 dioctahedral structure.

The phyllosilicate slabs used for the interface simulations consisted of four 2:1 layers with surface areas of approximately 30 Å × 30 Å and the basal surface was exposed on both faces of the slab. Except for pyrophyllite, cleaving the basal surface resulted in the slab top face with a full layer of interlayer cations and a bottom face without any interlayer cations; half of the surface cations were, therefore, moved from the top face to the bottom face to remove the dipole normal to the surface thus created. This resulted in surface configurations with rows of cavities along the [100] direction that were either empty or full and alternating empty and full rows of cavities along the [010] direction. Top views of the phyllosilicate slabs are shown in Figure 1.

The direction normal to the surface was extended to create a gap of approximately 40 Å, which was filled with approximately 1150 water molecules. To equilibrate the interfaces, a 1-ns MD simulation was first run with the mineral slab fixed. Then, another 1-ns MD simulation (with an initial equilibration period of 100 ps) was run, with all atoms free to move, to determine the average atomic density profiles. The final configuration from this simulation was used as the starting point for calculating the adsorption free energy profiles described below. Because of the small layer charge of illite, some of the surface K^+ ions were observed to desorb from the surface; therefore, a second set of simulations was performed for this mineral, whereby the surface K^+ ions were tethered to the original position using a harmonic potential in order to ensure adequate comparison with the other phyllosilicate surfaces, for which the surface cations (K^+ or Ca^{2+}) remained absorbed. A series of simulations was performed in which the tether force constant was decreased until the minimal value required to retain all K^+ ions at the surface during a 1-ns MD simulation was determined to be 0.05 eV/ $Å^2$. Results obtained with and without the harmonic tether will be presented and contrasted.

Potential of mean force calculations

Free energy profiles of Cs adsorption on the basal surface of the six model phyllosilicates were obtained from potential of mean force (PMF) calculations. Following this approach, a series of MD simulations were carried out whereby Cs^+ was constrained at a height z above the surface but was free to move in the plane parallel to the surface. In each simulation, Cs^+ was initially placed directly above a six-membered ring cavity not occupied by a charge-compensating surface cation and the nearest water molecule was removed to avoid overlaps. The free energy difference, ΔA, between Cs^+ at a height z and in the middle of the water slab (*i.e.* at height z_0) was then obtained by integrating the

Table 3. Chemical formulae, structures, and magnitude and location of the layer charge of the model phyllosilicates studied in this work.

Mineral	Formula	Structure	— Layer charge — Magnitude	Location
Pyrophyllite	$[Al_2]_{oct.}[Si_4]_{tet.}O_{10}(OH)_2$	2:1 dioctahedral	0	–
Illite	$K[Al_4]_{oct.}[Si_7Al]_{tet.}O_{20}(OH)_4$	2:1 dioctahedral	0.5	tetrahedral
Muscovite	$K[Al_2]_{oct.}[Si_3Al]_{tet.}O_{10}(OH)_2$	2:1 dioctahedral	–1	tetrahedral
Phlogopite	$K[Mg_3]_{oct.}[Si_3Al]_{tet.}O_{10}(OH)_2$	2:1 trioctahedral	–1	tetrahedral
Celadonite	$K[MgAl]_{oct.}[Si_4]_{tet.}O_{10}(OH)_2$	2:1 dioctahedral	–1	octahedral
Margarite	$Ca[Al_2]_{oct.}[Si_2Al_2]_{tet.}O_{10}(OH)_2$	2:1 dioctahedral	–2	tetrahedral

https://doi.org/10.1346/CCMN.2016.0640405 Published online by Cambridge University Press

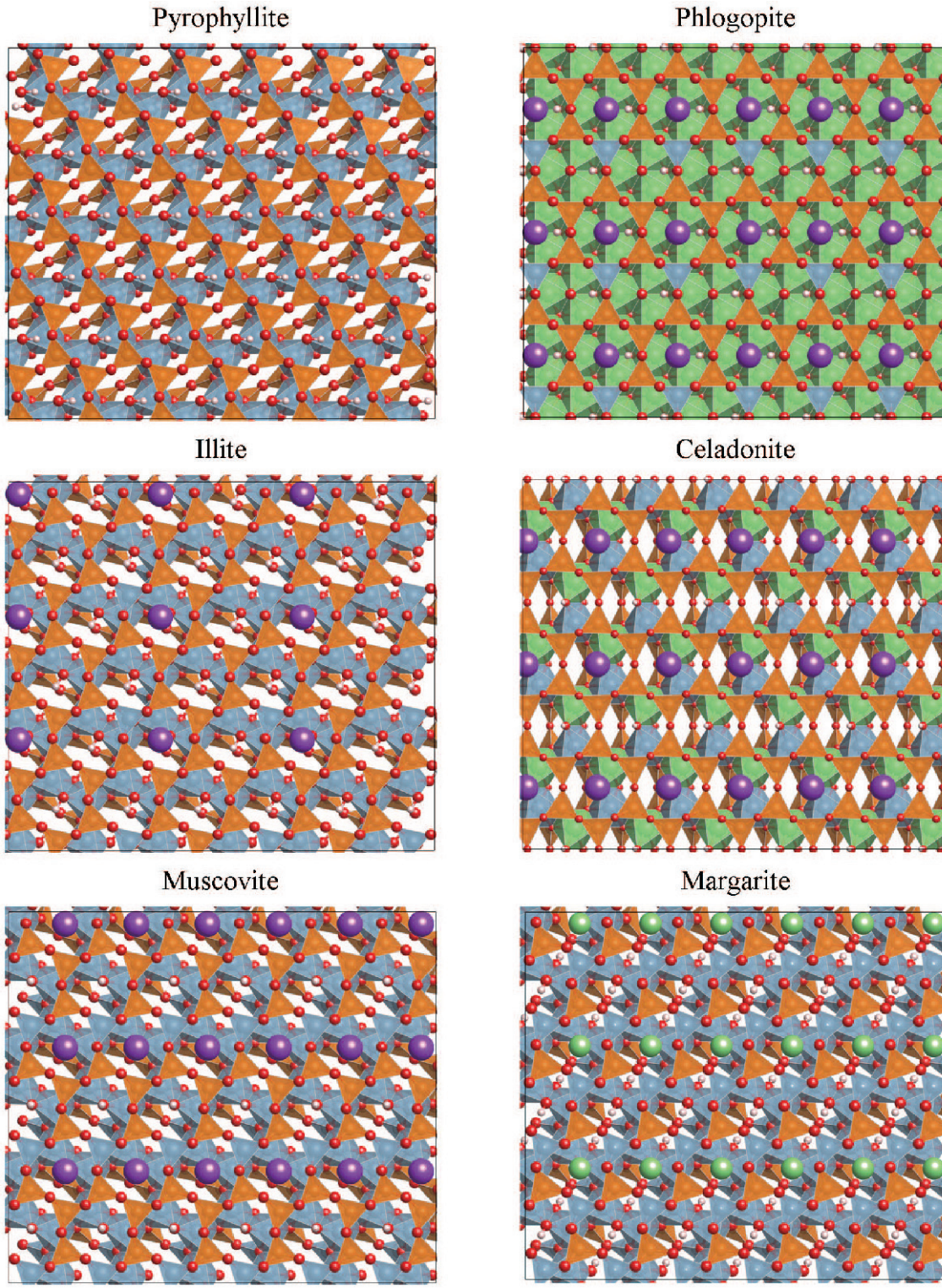

Figure 1. Top views of the basal surface of the six phyllosilicate minerals considered in this work. (Grayscale appearance). SiO_4 tetrahedra are shown as dark orange (dark gray) tetrahedra, AlO_4 tetrahedra as blue (light gray) tetrahedra, AlO_6 octahedra as blue (light gray) octahedra, MgO_6 octahedra as green (light) octahedra, O atoms as small red (dark) spheres, H atoms as small white (light) spheres, K atoms as purple (dark) spheres, and Ca atoms as large green (light) spheres. This figure was generated using VESTA (Momma and Izumi, 2011).

https://doi.org/10.1346/CCMN.2016.0640405 Published online by Cambridge University Press

average force in the direction perpendicular to the surface, f_z, acting on Cs^+ from z_0 to z:

$$\Delta A(z) = A(z) - A(z_0) = \int_{z_0}^{z} \langle f_z(z) \rangle dz \quad (1)$$

To construct the free energy profile for Cs^+ adsorption at the basal surface of each phyllosilicate, 80 constrained MD simulations were performed along the normal to the surface at 0.2 Å intervals. Each simulation was run for 300 ps following a 100 ps equilibration period. The PMF simulations represent the adsorption of Cs^+ on an otherwise neutral surface in the infinite dilution limit.

Thermodynamic integration calculations

Thermodynamic integrations were carried out to calculate hydration free energies. The calculations proceeded in two stages: (1) the solvation cavity was grown by varying the short-range potential parameters in 12 intervals, whereby the dependence of the Hamiltonian H on the mixing parameter λ was defined as $H_\lambda = f(\lambda)H$, where $f(\lambda) = 1 - (1 - \lambda)^k$ and k equals 6, and the 12 values of λ defined by Horinek *et al.* (2009) were used; and (2) the ion was slowly charged, with the short-range parameters set to the full values, in 11 intervals, whereby the dependence of the Hamiltonian on λ was set to be linear $f(\lambda) = \lambda$ and where λ was varied from 0.0 to 1.0 in 0.1 intervals. Two sets of corrections were applied to allow comparison with experimental data (Hummer *et al.*, 1997a, 1997b; Kastenholz and Hünenberg, 2006a, 2006b). The first set of corrections accounted for the system finite size and periodicity effects on water polarization. The second set of corrections accounted for the difference between the gas phase experimental and theoretical reference states. The calculated hydration free energies were based on the P-summation scheme.

RESULTS

Bulk phyllosilicates

A 1-ns NPT MD simulation was first carried out for each of the six model phyllosilicates. The cell angles were set to the experimental values and kept constant throughout the simulations. The resulting cell edge lattice parameters (Table 4) showed that the CLAYFF model yielded a good structural description of the phyllosilicates of interest with all lattice parameters reproduced within 1.5%. One exception was margarite, for which the CLAYFF model predicted lattice parameters 2.8% shorter than observed experimentally. Because the main difference between margarite and the other phyllosilicates was interlayer Ca^{2+} ions, this difference was expected to be due to model parameters that overestimated the bonding strength of Ca to other atom types.

Structure, thermodynamics, and kinetics of Cs hydration

As a reference for the simulations of Cs adsorption, a 1-ns NPT MD simulation of a single Cs^+ ion in a simulation cell containing 511 H_2O molecules was carried out. The mean Cs-water oxygen distance determined from this simulation was 3.08 Å, in excellent agreement with the distance determined by Mähler and Persson (2012) from large-angle X-ray scattering (3.07 Å). The first minimum in the Cs-water oxygen radial distribution function was found at 4.05 Å and was used as the first hydration shell outer boundary. The instantaneous number of water molecules in the first hydration shell (*i.e.* Cs coordination number) varied from 5 to 14 with coordination numbers 8, 9, and 10 being the most likely. The most likely coordination numbers (8, 9, and 10) had at least a 20% probability with a summed probability of about 75% (*i.e.* Cs adopted an 8, 9, or 10 coordination number in 75% of the calculated configurations). The average coordination number was 9.2. The residence time of H_2O molecules in the first hydration shell was 5.7 ps, which was close to the residence time of H_2O molecules in the first coordination shell of other H_2O molecules (~4 ps). As determined from previous molecular simulations (Schwenk *et al.*, 2004), these results indicated that Cs-water interactions were weak, which resulted in a large, weakly bound single hydration shell that underwent very rapid exchange. Thermodynamic integration yielded a hydration free energy for Cs^+ of −237 kJ/mol, *i.e.* a 5%

Table 4. Experimental and calculated lattice parameters of the six model phyllosilicates considered in this work.

Mineral	Calculated			Experimental/*Ab initio*			Δ
	a (Å)	*b* (Å)	*c* (Å)	*a* (Å)	*b* (Å)	*c* (Å)	(%)
Pyrophyllite	5.191	9.020	9.404	5.160[a]	8.966[a]	9.347[a]	+0.6
Illite	5.190	9.001	10.046	5.27[b]	9.14[b]	10.2[b]	-1.5
Muscovite	5.159	8.957	20.004	5.177[c]	8.987[c]	20.072[c]	-0.3
Phlogopite	5.273	9.129	10.070	5.32[d]	9.21[d]	10.16[d]	-0.9
Celadonite	5.180	8.946	9.994	5.223[e]	9.020[e]	10.077[e]	-0.8
Margarite	4.960	8.580	18.608	5.104[f]	8.829[f]	19.148[f]	-2.8

[a] Lee and Guggenheim (1981); [b] Hernández-Laguna *et al.* (2006) (*ab initio*); [c] Liang and Hawthorne (1996); [d] Pabst (Pabst, 1955); [e] Drits *et al.* (2010); [f] Guggenheim and Bailey (1975).

https://doi.org/10.1346/CCMN.2016.0640405 Published online by Cambridge University Press

underestimation of the experimental value reported by Marcus (1991) (−250 kJ/mol). For comparison, the calculated hydration free energy of K^+, which was present at the surface of four of the six model phyllosilicates, was underestimated by 7% (−273 kJ/mol *vs.* −295 kJ/mol).

Interfacial water structures

Figure 2 shows the interfacial density profiles (lattice oxygens, water oxygens, and surface K or Ca ions) for the six model phyllosilicates. The plane of the surface was used as the zero distance and was defined as the plane that passes through the topmost Si tetrahedral sites. Although the interactions between water and the pyrophyllite surface were weak, an interfacial structure was induced by the presence of the solid surface. Water molecules in the first interfacial peak formed hydrogen bonds with other water molecules and occasionally donated hydrogen bonds to surface oxygens, in agreement with the results obtained by Greathouse and Cygan (2006). Illite exhibited a water density profile similar to that of pyrophyllite. In addition, a small and fairly broad peak due to the surface K ions was observed when a harmonic tether was used. In the absence of the harmonic tether, the magnitude of the peak due to the surface K ions decreased and a very weak outer-sphere peak appeared. Additionally, water molecules occupied surface sites left vacant by the desorbed K ions, leading to an increase in the magnitude of the first interfacial water peak. The interfacial density profiles were otherwise identical.

The interfacial water structure at the muscovite surface was more defined. The first, smaller peak corresponds to water molecules that adsorbed directly above half of the six-membered siloxane ring cavities (with the other half occupied by K ions) and that donated hydrogen bonds to surface oxygens. The second and third interfacial water peaks correspond to water molecules that interacted predominantly with species in the six-membered ring cavities (water molecules under the first water interfacial peak and surface K ions); although a small proportion of water molecules also donated hydrogen bonds to surface oxygens. The calculated interfacial water structure was consistent with that obtained by Wang *et al.* (2005) and Sakuma

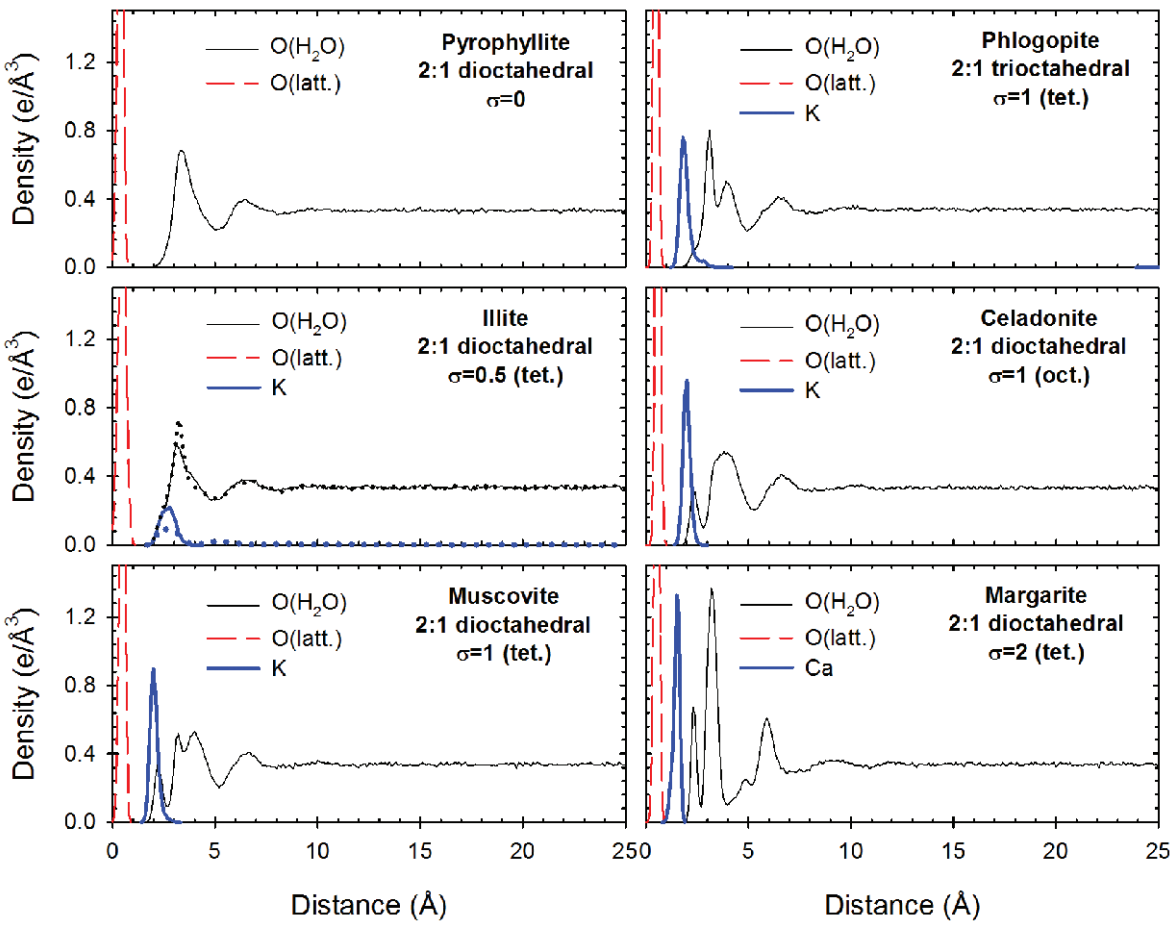

Figure 2. Interfacial density profiles for the six model phyllosilicates. σ is the permanent layer charge. For illite, the profiles obtained with and without a harmonic tether applied to the surface K ions are shown with solid and dashed lines, respectively.

https://doi.org/10.1346/CCMN.2016.0640405 Published online by Cambridge University Press

and Kawamura (2009) in previous molecular dynamics simulations. The peak due to surface K ions was narrower and more intense than that at the illite-water interface due to the increased layer charge and number of surface K ions.

The interfacial water structure at the phlogopite surface was similar to that at the muscovite surface, except that, due the trioctahedral structure, the hydroxide ions of the octahedral sheet were positioned higher towards the surface in the cavities of the six-member rings, which had the effect of pushing out the water molecules located in the cavity sites and causing a significant reduction in the magnitude of the first water peak. The peak due to surface K ions remained similar, however.

The interfacial water structure at the celadonite surface was also similar to that at the muscovite surface. Because of the lack of tetrahedral substitutions, average hydrogen bonds to surface oxygens were longer than at the muscovite–water and phlogopite–water interfaces, which caused the second and third water layers to merge into a single, broad peak. At the margarite–water interface, the increased layer charge meant that both water molecules and Ca ions were more strongly bound at the surface, resulting in much narrower interfacial peaks. The stronger interactions between water molecules and surface Ca ions, relative to those with surface K ions, caused the water molecules in the second and third layers to adopt more rigid orientations, with the oxygen atoms towards the surface Ca ions and hydrogen bond interactions with water molecules in the surface cavities or with surface oxygens. This led to a tall and narrow second water interfacial peak and a significant trough between approximately 4 and 5.5 Å above the surface.

Free energy profiles of Cs adsorption

The potentials of mean force for Cs^+ adsorption on the basal surface of the six model phyllosilicates were calculated (Figure 3) together with the Cs^+ coordination numbers with water oxygens and oxygens of the mineral lattice (Figure 3). For pyrophyllite, as Cs^+ approached the surface, a slight increase in its coordination number with water molecules was calculated at approximately 6 Å; but the free energy of adsorption as an outer-sphere complex was essentially zero within the uncertainties of this approach. As Cs^+ more closely approached the surface, hydration waters were replaced by lattice oxygens in the first coordination shell; however, no corresponding inner-sphere adsorption minimum was obtained and Cs adsorption on the basal surface of pyrophyllite was predicted to be unfavorable.

Cesium adsorption on the other five basal surfaces was predicted to be favorable. All five profiles were qualitatively similar with a very weakly favorable outer-sphere adsorption site, a free energy barrier for adsorption that corresponded with the height at which Cs^+ began to exchange hydration water for lattice oxygens, and a significant free energy minimum where Cs^+ was adsorbed as an inner-sphere complex. One exception was the Cs^+ adsorption as an outer-sphere complex on the illite basal surface in the absence of a harmonic tether acting on surface K ions, which was calculated to be unfavorable due to the presence of like-charged K^+ ions in outer-sphere positions.

Comparison of the inner-sphere free energy minima depths at the basal surface of pyrophyllite (unfavorable), illite (−7.2 and −5.0 kJ/mol with and without harmonic tether on surface K^+ ions, respectively), muscovite (−19.4 kJ/mol), and margarite (−39.3 kJ/mol) demonstrated that, for a given layer structure and layer charge location, the adsorption free energy became more favorable with increasing layer charge.

The inner-sphere free energy minima depths at the muscovite (−19.4 kJ/mol) and phlogopite (−8.7 kJ/mol) basal surfaces showed that, for a given layer charge magnitude and location, the octahedral sheet structure affected Cs adsorption, whereby the free energy minimum depth for a 2:1 trioctahedral phyllosilicate was approximately half that on the corresponding 2:1 dioctahedral mineral. This difference was explained by the mean inter-atomic distances and the Cs^+ coordination numbers when adsorbed as an inner-sphere complex (Table 5). To allow for an accurate determination of the mean inter-atomic distances, additional 1-ns MD simulations were carried out for Cs free of constraints and initially positioned in the inner-sphere configuration determined from the PMF calculations. When adsorbed at the phlogopite basal surface (Figure 4), Cs^+ was positioned much closer to the octahedral sheet hydroxide ion hydrogen atom than when Cs^+ was adsorbed at the muscovite surface (Figure 4), leading to greater electrostatic repulsion (Table 5).

The inner-sphere free energy minima depth at the muscovite (−19.4 kJ/mol) and celadonite (−29.3 kJ/mol) basal surfaces indicated that, for a given layer charge magnitude and octahedral sheet structure, layer charge location can affect Cs^+ adsorption. At the muscovite surface, Cs was slightly shifted towards the more negatively charged bridging oxygen atoms with tetrahedral substitution, resulting in shorter Cs−K distances than at the celadonite surface (Table 5). Additionally, the calculated Cs position was farther away from the hydroxide ion oxygen atom directly below the cavity of the six-membered ring (Table 5). Both aspects could have contributed to inner-sphere complex destabilization at the muscovite surface relative to the celadonite surface and led to the observed reduction in the magnitude of the free energy minimum.

DISCUSSION

A close-up of the adsorption profiles revealed the presence of very weakly adsorbed outer-sphere complexes (Figure 5). All six minerals showed an outer-

https://doi.org/10.1346/CCMN.2016.0640405 Published online by Cambridge University Press

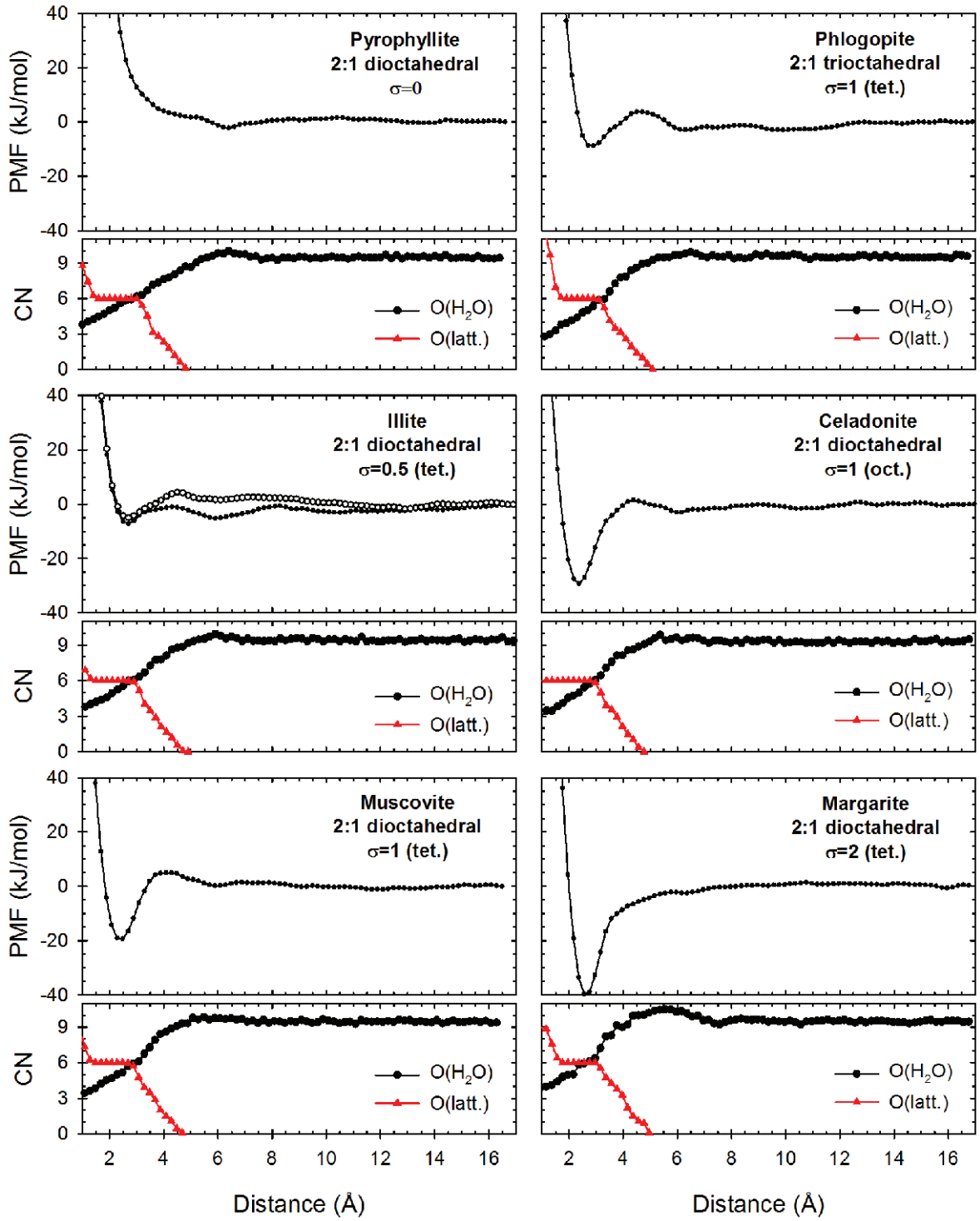

Figure 3. Potentials of mean force (PMF) for Cs^+ adsorption on the basal surface of the six model phyllosilicates. Also shown are the coordination numbers (CN) of Cs^+ with water oxygens and oxygens of the phyllosilicate lattice. σ is the permanent layer charge. For illite, the PMF obtained with and without a harmonic tether applied to the surface K ions are shown with solid and empty circles, respectively (the calculated coordination numbers were identical in both cases and only the case in which the harmonic tether was applied is shown).

https://doi.org/10.1346/CCMN.2016.0640405 Published online by Cambridge University Press

Table 5. Mean inter-atomic distances between Cs and other atom types for Cs^+ adsorbed as an inner-sphere complex. Coordination numbers are shown in parentheses.

Mineral	Tetrahedral sheet						Octahedral sheet			
	O*	K/Ca	Ob	Obts	St	At	Oh/Ohs	Ho	Ao	Mgo/Mgh
Illite	3.15 (×5.8)	4.65 (×2.0)	3.45 (×3.9)	3.15 (×2.0)	3.95 (×5.0)	3.85 (×1.0)	4.45 (×1.0)	4.65 (×1.0)	5.65 (×1.9)	–
Muscovite	3.15 (×5.3)	4.85 (×4.0)	3.15 (×4.0)	3.05 (×2.0)	3.85 (×5.0)	3.75 (×1.0)	4.25 (×1.0)	4.55 (×1.0)	5.45 (×2.0)	–
Phlogopite	3.05 (×5.2)	5.15 (×4.0)	3.25 (×4.0)	3.05 (×2.0)	3.95 (×5.0)	3.75 (×1.0)	3.95 (×1.0)	3.45 (×1.0)	–	5.65 (×3.0)
Celadonite	3.15 (×5.0)	5.15 (×4.0)	3.15 (×6.0)	–	3.85 (×6.0)	–	3.95 (×1.0)	4.35 (×1.0)	5.45 (×1.1)	5.35 (×1.0)
Margarite	3.15 (×6.2)	4.95 (×4.0)	–	3.05 (×6.0)	3.75 (×3.0)	3.75 (×3.0)	4.15 (×1.0)	4.25 (×1.0)	5.55 (×2.1)	–

The reader is referred to Table 1 for the symbol definitions.

sphere free energy minimum between 5.9 and 6.4 Å. In addition, illite, muscovite, phlogopite, and celadonite showed a second, also weakly adsorbed outer-sphere complex. The free energy minima corresponding to these complexes were very broad and extended from approximately 8–9 Å to 12–13 Å for phlogopite and celadonite and to up to 15–16 Å for illite and muscovite. These results are consistent with reports of weakly bound "extended" outer-sphere complexes at the muscovite (001) surface, which were first discovered based on X-ray reflectivity measurements (Lee *et al.*, 2010). Although these measurements were for more strongly hydrated divalent cations, some cation density was observed in this extended region for Rb^+, which is also weakly hydrated, and the very shallow minima obtained in this work would likely be below the detection limit of the experiments.

Although outer-sphere complexes were predicted to be present, the potential of mean force calculations clearly showed that Cs^+ adsorption was predominantly inner-sphere at the basal surfaces of the model phyllosilicates, with the exception of pyrophyllite. This finding is in agreement with X-ray reflectivity measurements of Lee *et al.* (2012; 2013), which demonstrated that, as the adsorbed alkali cation hydration free-energy decreased in magnitude, inner-sphere adsorption became progressively favored over outer-sphere adsorption. For muscovite, the partition between inner- and outer-sphere complexes (K_{IO}) can be obtained from the ratio of the PMF profile integrals over the inner-sphere (up to 4.3 Å) and outer-sphere (from 4.3 Å to 15.9 Å to include the 'extended' outer-sphere region) regions. This yielded a value of log K_{IO} of 2.0, which corresponded to a free energy difference of −11.5 kJ/mol, which is in relatively good agreement with the experimental values of Lee *et al.* (2013) (log K_{IO} = 1.5; ΔG_{IO} = −8.4 kJ/mol) obtained for 0.003 molal CsCl. Also in good agreement with the experimental results of Lee *et al.* (2013) was the calculated free energy minimum of −19.4 kJ/mol for Cs^+ adsorbed as an inner-sphere complex on the muscovite surface compared to −21.2 kJ/mol obtained experimentally from the Langmuir isotherm approach.

In the MD simulation where Cs^+ was unconstrained, the Cs density peak was 2.0 Å above the muscovite surface compared to 2.26 ± 0.01 Å, 2.15 ± 0.09 Å, and 2.16 ± 0.02 Å obtained from X-ray reflectivity measurements (Lee *et al.*, 2012; Schlegel *et al.*, 2006) for 0.003 m, 0.01 m, and 0.5 m CsCl solutions and 2.0–2.2 Å and 2.1 Å from the molecular simulations of Meleshyn (2008) and Sakuma and Kawamura (2011), respectively. Unlike the density and PMF profiles, these positions were determined with respect to the average height of the topmost surface oxygens for consistency with the notation used by Lee *et al.* (2012) and Schlegel *et al.* (2006). The Cs density peaks were at 2.2, 2.1, 1.9, and 2.1 Å above the illite, phlogopite, celadonite, and margarite surfaces, respectively.

https://doi.org/10.1346/CCMN.2016.0640405 Published online by Cambridge University Press

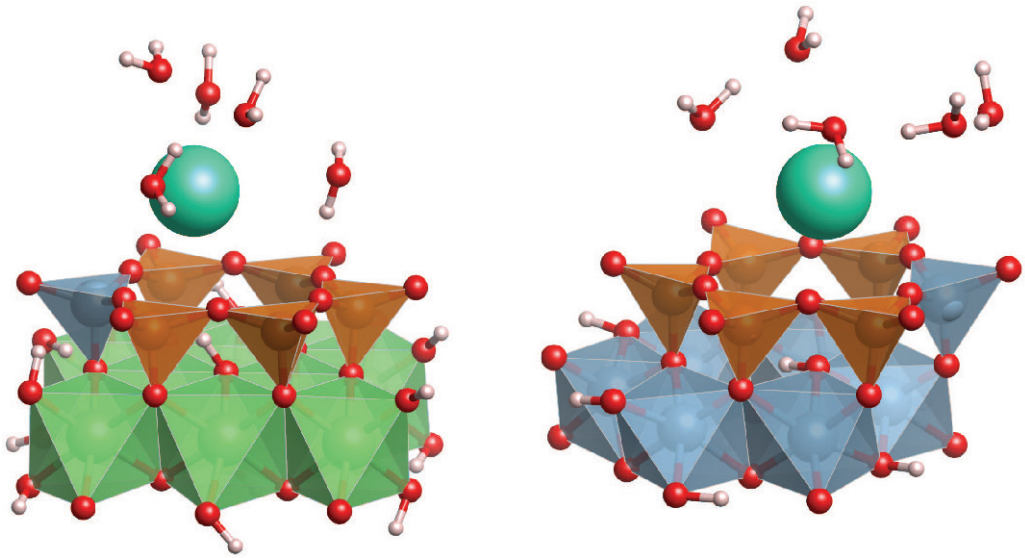

Figure 4. Snapshots from the simulations of Cs^+ adsorbed on phlogopite (left) and muscovite (right). The color scheme (grayscale) used was the same as in Figure 1. The Cs atom is shown as a large green (light) sphere. Only water molecules in the first hydration shell of Cs^+ are shown. This figure was generated using VESTA (Momma and Izumi, 2011).

Overall, comparisons with experimental data and previous molecular simulations of Cs^+ adsorption at the muscovite (001) surface showed that the Cs^+ structure at the interface, the Cs^+ adsorption thermodynamics, and the partition of Cs^+ between inner-sphere and outer-sphere sites were well described by the atomistic model. Turning to the other phyllosilicates, the MD simulations predicted similar Cs^+ adsorption properties to those observed for muscovite. For the four minerals with a 2:1 dioctahedral structure and tetrahedral sheet layer charge, a linear relationship (Figure 6) exists between layer charge magnitude and the free energy minimum of

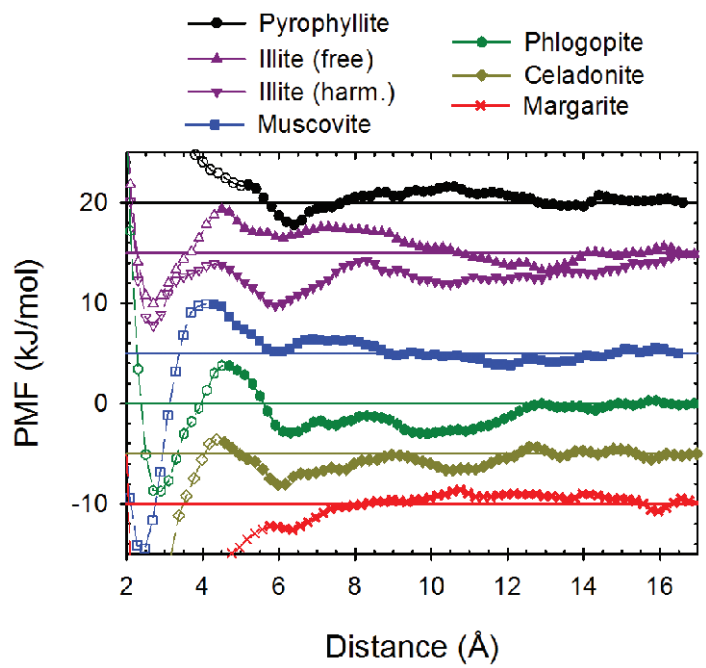

Figure 5. Close-up of the outer-sphere region of the potentials of mean force (PMF) for Cs^+ adsorption on the basal surface of the six model phyllosilicates. Profiles were shifted along the *y* axis for clarity. The inner-sphere region is shown with empty circles and dashed lines.

https://doi.org/10.1346/CCMN.2016.0640405 Published online by Cambridge University Press

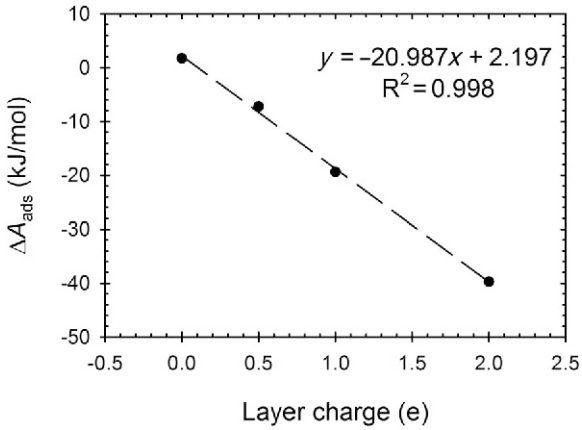

Figure 6. Free energy of adsorption of Cs^+ as an inner-sphere complex at the basal surfaces of 2:1 dioctahedral phyllosilicates as a function of the permanent layer charge. Permanent layer charge is located in the tetrahedral sheet and is the result of Al substitution for Si.

adsorption as an inner-sphere Cs^+ complex (for pyrophyllite, the minimum free energy within the inner-sphere region, *i.e.* within 5.0 Å, was used; for illite, simulations with the harmonic tether were used to isolate the effect of permanent charge magnitude) using a large gradient (*i.e.* layer charge *vs.* free energy minimum) of ~20 kJ/mol/*e*. This result suggests that the inner-sphere adsorption sites at the basal surface of these four minerals were sufficiently similar so that adsorption free energy differences were dominated by the electrostatic interactions between Cs^+ and the permanent layer charge.

CONCLUSION

The MD simulations were performed to determine the dependence of Cs^+ adsorption thermodynamics at 2:1 phyllosilicate mineral basal surfaces on a series of structural properties. The MD simulations showed good agreement with experiment with respect to the structure of the phyllosilicate minerals of interest, the energetics and structure of Cs^+ in water, and the adsorption geometry and thermodynamics of Cs^+ at the muscovite (001) surface. This good agreement validated the model used in this work (CLAYFF with the flexible SPC water model). The PMF calculations of Cs^+ adsorption on six model phyllosilicates indicated that layer charge magnitude and location, as well as octahedral sheet structure, all played an important role in determining the Cs^+ propensity for inner-sphere complex adsorption. In contrast, predicted Cs^+ adsorption as an outer-sphere complex was very weak and independent of these factors. Importantly, the Cs^+ adsorption free energy varied linearly with the layer charge magnitude, when other structural factors were identical. In other cases, where layer charge magnitude was kept constant, the adsorption site geometry was an important influence on the adsorption free energy, particularly the hydroxide ion position below the cavity of the six-membered ring and the other surface cation positions. Finally, the free energy barrier for Cs^+ adsorption as an inner-sphere complex was associated with the removal of the waters of hydration around Cs^+ and was calculated to be low and, therefore, not rate limiting. This can be attributed to the weak binding between Cs^+ and water molecules in aqueous solution.

ACKNOWLEDGMENTS

This research was supported by the Japan Atomic Energy Agency.

REFERENCES

Cygan, R.T., Liang, J.-J., and Kalinichev, A.G. (2004) Molecular models of hydroxide, oxyhydroxide, and clay phases and the development of a general force field. *Journal of Physical Chemistry B*, **108**, 1255–1266.

Drits, V.A., Zviagina, B.B., McCarty, D.K., and Salyn, A.L. (2010) Factors responsible for crystal-chemical variations in the solid solutions from illite to aluminoceladonite and from glauconite to celadonite. *American Mineralogist*, **95**, 348–361.

Ewald, P.P. (1921) Die Berechnung Optischer und Elektrostatischer Gitterpotentiale. *Annalen der Physik*, **64**, 253–287.

Geatches, D.L. and Wilcox, J. (2014) *Ab initio* investigations of dioctahedral interlayer-deficient mica: modelling 1 *M* polymorphs of illite found within gas shale. *European Journal of Mineralogy*, **26**, 127–144.

Greathouse, J.A. and Cygan, R.T. (2006) Water structure and aqueous uranyl(VI) adsorption equilibria onto external surfaces of beidellite, montmorillonite, and pyrophyllite: Results from molecular simulations. *Environmental Science & Technology*, **40**, 3865–3871.

Guggenheim, S. and Bailey, S.W. (1975) Refinement of the margarite structure in subgroup symmetry. *American Mineralogist*, **60**, 1023–1029.

Hernández-Laguna, A., Escamilla-Roa, E., Timón, V., Dove, M.T., and Sainz-Díaz, I.C. (2006) DFT study of the cation arrangements in the octahedral and tetrahedral sheets of dioctahedral 2:1 phyllosilicates. *Physics and Chemistry of Minerals*, **33**, 655–666.

Hoover, W.G. (1985) Canonical dynamics – equilibrium phase-space distributions. *Physical Review A*, **31**, 1695–1697.

Horinek, D., Mamatkulov, S.I., and Netz, R.R. (2009) Rational design of ion force fields based on thermodynamic solvation properties. *Journal of Chemical Physics*, **130**, 124507.

Hummer, G., Pratt, L.R., and Garcia, A.E. (1997a) Ion sizes and finite-size corrections for ionic-solvation free energies. *Journal of Chemical Physics*, **107**, 9275–9277.

Hummer, G., Pratt, L.R., Garcia, A.E., Berne, B.J., and Rick, S.W. (1997b) Electrostatic potentials and free energies of solvation of polar and charged molecules. *Journal of Physical Chemistry B*, **101**, 3017–3020.

Kastenholz, M.A. and Hünenberg, P.H. (2006a) Computation of methodology-independent ionic solvation free energies from molecular simulations. I. The electrostatic potential in molecular liquids. *Journal of Chemical Physics*, **124**, 124106.

Kastenholz, M.A. and Hünenberg, P.H. (2006b) Computation of methodology-independent ionic solvation free energies from molecular simulations. II. The hydration free energy of

https://doi.org/10.1346/CCMN.2016.0640405 Published online by Cambridge University Press

the sodium cation. *Journal of Chemical Physics*, **124**, 224501.

Kato, H., Onda, Y., and Teramage, M. (2012) Depth distribution of ^{137}Cs, ^{134}Cs, and ^{131}I in soil profile after Fukushima Dai-ichi nuclear power plant accident. *Journal of Environmental Radioactivity*, **111**, 59–64.

Kozai, N., Ohnuki, T., Arisaka, M., Watanabe, M., Sakamoto, F., Yamasaki, S., and Jiang, M. (2012) Chemical states of fallout radioactive Cs in the soils deposited at Fukushima Daiichi Nuclear Power Plant accident. *Journal of Nuclear Science and Technology*, **49**, 473–478.

Lee, J.H. and Guggenheim, S. (1981) Single crystal X-ray refinement of pyrophyllite-1 TC. *American Mineralogist*, **66**, 350–357.

Lee, S.-S., Fenter, P., Park, C., Sturchio, N.C., and Nagy, K.L. (2010) Hydrated cation speciation at the muscovite (001)-water interface. *Langmuir*, **26**, 16647-16651.

Lee, S.-S., Fenter, P., Nagy, K.L., and Sturchio, N.C. (2012) Monovalent ion adsorption at the muscovite (001)-solution interface: Relationships among ion coverage and speciation, interfacial water structure, and substrate relaxation. *Langmuir*, **28**, 8637–8650.

Lee, S.-S., Fenter, P., Nagy, K.L., and Sturchio, N.C. (2013) Changes in adsorption free energy and speciation during competitive adsorption between monovalent cations at the muscovite (001)-water interface. *Geochimica et Cosmochimica Acta*, **123**, 416–426.

Liang, J.-J. and Hawthorne, F.C. (1996) Rietveld refinement of micaceous materials: Muscovite-2M_1, a comparison with single-crystal structure refinement. *Canadian Mineralogist*, **34**, 115–122.

Mähler, J. and Persson, I. (2012) A study of the hydration of the alkali metal ions in aqueous solution. *Inorganic Chemistry*, **51**, 425–438.

Marcus, Y. (1991) Thermodynamics of solvation on ions. Part 5. – Gibbs free energy of hydration at 298.15 K. *Journal of the Chemical Society - Faraday Transactions*, **87**, 2995–2999.

Melchionna, S., Ciccotti, G., and Holian, B.L. (1993) Hoover NPT Dynamics for Systems Varying in Shape and Size. *Molecular Physics*, **78**, 533–544.

Meleshyn, A. (2008) Aqueous solution structure at the cleaved mica surface: Influence of K^+, H_3O^+, and Cs^+ adsorption. *Journal of Physical Chemistry C*, **112**, 20018-20026.

Momma, K. and Izumi, F. (2011) VESTA 3 for three-dimensional visualization of crystal, volumetric and morphology data. *Journal of Applied Crystallography*, **44**, 1272–1276.

Okumura, M., Nakamura, H., and Machida, M. (2013) Mechanism of strong affinity of clay minerals to radioactive cesium: First-principles calculation study for adsorption of cesium at frayed edge sites in muscovite. *Journal of the Physical Society of Japan*, **82**, 033802.

Okumura, M., Nakamura, H., and Machida, M. (2014) Energetics of atomic level serial ion exchange for cesium in micaceous clay minerals. *Clay Science*, **18**, 53–61.

Pabst, A. (1955) Redescription of the single layer structure of the micas. *American Mineralogist*, **40**, 967–974.

Qin, H., Yokoyama, Y., Fan, Q., Iwatani, H., Tanaka, K., Sakaguchi, A., Kanai, Y., Zhu, J., Onda, Y., and Takahashi, Y. (2012) Investigation of cesium adsorption on soil and sediment samples from Fukushima Prefecture by sequential extraction and EXAFS technique. *Geochemical Journal*, **46**, 297–302.

Rosso, K.M., Rustad, J.R., and Bylaska, E.J. (2001) The Cs/K exchange in muscovite interlayers: An *ab initio* treatment. *Clays and Clay Minerals*, **49**, 500–513.

Sakuma, H. and Kawamura, K. (2009) Structure and dynamics of water on muscovite mica surfaces. *Geochimica et Cosmochimica Acta*, **73**, 4100–4110.

Sakuma, H. and Kawamura, K. (2011) Structure and dynamics of water on Li^+-, Na^+-, K^+-, Cs^+-, H_3O^+-exchanged muscovite surfaces: A molecular dynamics study. *Geochimica et Cosmochimica Acta*, **75**, 63–81.

Schlegel, M.L., Nagy, K.L., Fenter, P., Cheng, L., Sturchio, N.C., and Jacobsen, S.D. (2006) Cation sorption on the muscovite (001) surface in chloride solutions using high-resolution X-ray reflectivity. *Geochimica et Cosmochimica Acta*, **70**, 3549–3565.

Schwenk, C.F., Hofer, T.S., and Rode, B.M. (2004) "Structure breaking" effect of hydrated Cs^+. *Journal of Physical Chemistry A*, **108**, 1509–1514.

Smith, W. and Forester, T.R. (1996) DL_POLY_2.0: A general purpose parallel molecular dynamics simulation package. *Journal of Molecular Graphics*, **14**, 136–141.

Tanaka, K., Takahashi, Y., Sakaguchi, A., Umeo, M., Hayakawa, S., Tanida, H., Saito, T., and Kanai, Y. (2012) Vertical profiles of iodine-131 and cesium-137 in soils in Fukushima Prefecture related to the Fukushima Daiichi Nuclear Power Station Accident. *Geochemical Journal*, **46**, 73–76.

Wang, J., Kalinichev, A.G., Kirkpatrick, R.J., and Cygan, R.T. (2005) Structure, energetics, and dynamics of water adsorbed on the muscovite (001) surface: A molecular dynamics simulation. *Journal of Physical Chemistry B*, **109**, 15893-15905.

(*Received 29 October 2015; revised 12 May 2016; Ms. 1059; AE: Xiandong Liu*)